I&EC research
Industrial & Engineering Chemistry Research

Article

pubs.acs.org/IECR

Synthesis and Characterization of γ-Fe_2O_3 for H_2S Removal at Low Temperature

Guan Huang,[†] Enyun He,[†] Zhongde Wang,[†] Huiling Fan,*[,†] Ju Shangguan,[†] Eric Croiset,[§] and Zhongwei Chen[§]

[†]State Key Laboratory of Coal Science and Technology, Co-founded by Shanxi Province and the Ministry of Science and Technology, Institute for Chemical Engineering of Coal, Taiyuan University of Technology, West Yingze Street Number 79, Taiyuan 030024, People's Republic of China

[§]Department of Chemical Engineering, University of Waterloo, 200 University Avenue West, Waterloo, Ontario N2L3G1, Canada

Supporting Information

ABSTRACT: The performance of γ-Fe_2O_3 as sorbent for H_2S removal at low temperatures (20−80 °C) was investigated. First, γ-Fe_2O_3/SiO_2 sorbents with a three-dimensionally ordered macropores (3DOM) structure were successfully prepared by a colloidal crystal templating method. Then, the performance of the γ-Fe_2O_3-based material, e.g., reference γ-Fe_2O_3 and 3DOM γ-Fe_2O_3/SiO_2 sorbents, for H_2S capture was compared with that of α-Fe_2O_3 and the commercial sorbent HXT-1 (amorphous hydrated iron oxide). The results show that γ-Fe_2O_3 has an enhanced activity compared to that of HXT-1 for H_2S capture at temperatures over 60 °C, whereas α-Fe_2O_3 has little activity. Because of the large surface area, high porosity, and nanosized active particles, 3DOM γ-Fe_2O_3/SiO_2 sorbent shows the best performance in terms of sulfur capacity and utilization. Moreover, it was found that moist conditions favor H_2S removal. Furthermore, it was found that the conventional regeneration method with air at high temperature was not ideal for the composite regeneration because of the transmission of some amount of γ-Fe_2O_3 to α-Fe_2O_3. However, simultaneous regeneration by adding oxygen in the feed stream allowed the breakthrough sulfur capacity of FS-8 to increase up to 79.1%, which was two times the value when there was no O_2 in the feed stream.

1. INTRODUCTION

Gaseous sulfur compounds are poisonous materials widely present in industrial feed gases such as natural, coal oven, and liquefied petroleum gases. The presence of a few parts per million of sulfur compounds can corrode equipment and pipelines, poison catalysts, and result in considerable economic losses. In addition, sulfur compounds in these fuel gases will ultimately be oxidized to sulfur dioxide that is then emitted into the atmosphere, causing health and environmental damage. Therefore, it is necessary to reduce the level of sulfur compounds in feed gases prior to their use.

As the most important contaminant sulfide, H_2S has received considerable attention. A number of materials that can effectively remove H_2S from feed gas streams at high temperatures have been identified, but the ultimate goal is to develop materials that can remove H_2S at low temperature because costs can be substantially reduced.[1] Amine solutions,[1,2] activated carbon,[1,3] molecular sieves,[4] as well as metals or mixed-metal oxides have been used for this purpose.[5−12] Garces et al.[5] investigated zinc oxide with a bimodal pore size distribution as a desulfurizing sorbent in a fixed-bed reactor at 60−400 °C. The results showed that the sorption capacity of the sorbent increased with sulfidation temperature and reached 87% of the theoretical maximum desulfurization at 400 °C. Song et al.[6] prepared a highly dispersed nano zinc oxide on the surface of reduced graphite oxide and used this composite for H_2S adsorption at ambient temperature. Carnes et al.[7] synthesized several nanocrystalline metal oxides by sol−gel or aerogel methods as materials for hydrogen sulfide removal. These nanocrystalline metal oxides were found to be considerably more reactive than commercial samples as a result of their higher surface areas and higher intrinsic reactivities. Efstathiou's group[8−10] developed novel Fe−Mn−Zn−Ti−O and various Zn−Ti-based mixed-metal oxides by sol−gel methods and tested them for low-temperature removal of H_2S from a gas mixture containing H_2, CO_2, and H_2O. It was found that the nominal chemical composition (metal atomic percent) of the solid adsorbent was an important factor in the particle size and morphology of the crystal phases formed. Different sulfidation mechanisms for each of the mixed-metal oxides were observed. Baird et al.[11−13] have investigated feroxyhyte (FeOOH), mixed cobalt−zinc oxides, and mixed cobalt−iron oxides as low-temperature H_2S adsorbents. Their results showed that the method used to prepare the precursors and the characteristics of the oxides were two key factors important for production of efficient low-temperature adsorbents of H_2S. Lattice diffusion played a major role in the rate-determining step. High surface area oxides provide additional H_2S adsorption sites, and lower-density oxides aid the diffusion of ions through the oxide bulk. A special form of iron oxide prepared by partially dehydrating α-FeOOH has been utilized for simultaneous removal of COS and H_2S, where COS is hydrolyzed to H_2S and then stabilized as iron sulfide on the surface of the iron oxide.[14] These examples from the literature indicate that high surface area and porosity, low density, and

Received: April 13, 2015
Revised: August 3, 2015
Accepted: August 6, 2015
Published: August 6, 2015

DOI: 10.1021/acs.iecr.5b01398
Ind. Eng. Chem. Res. 2015, 54, 8469−8478

nanosized particles are advantageous for metal oxide desulfurization.

Among the solid metal oxide sorbents, iron oxides are widely used to capture sulfur from industrial gases over a wide range of temperatures.[1] This feature is inherently due to the various forms of iron oxides, which, according to the literature, include oxides, hydroxides, or oxide-hydroxide forms.[15,16] Most iron oxides have the ability to capture sulfur, each being more suited to a different temperature range. For example, hematite (α-Fe_2O_3) is activated at 300−400 °C while hydrated iron oxides or hydroxides effectively remove H_2S at ambient temperature. The latter can be traced as the earliest sorbents for H_2S removal at ambient temperature.[1,16,17] However, little is known regarding the desulfurization behavior of maghemite (γ-Fe_2O_3). To the best of the authors' knowledge, the report from Gong et al.[18] is the only paper mentioning that γ-Fe_2O_3 is effective for sulfur removal at low temperatures. Maghemite is well-known for its wide application in magnetic recording and information storage devices.[19,20]

Maghemite occurs naturally in soils as a weathering product of magnetite or as a product of heating other Fe oxides. It exhibits an inverse spinel crystal structure, with vacancies in the cation sublattice. Each unit cell of maghemite contains 32 O^{2-} ions, 21 Fe^{3+} ions and 2 1/3 vacancies.[15,21−23] It is thermodynamically unstable and transforms to the most stable form, α-Fe_2O_3. The conventional commercial process for production of γ-Fe_2O_3 is a costly and cumbersome multistep procedure involving dehydroxylation of FeOOH, reduction of hematite, and controlled oxidation of Fe_3O_4.[15,24]

Recently, an iron oxide sorbent with a novel structure composed of three-dimensionally ordered macropores (3DOM) has been fabricated.[25] This 3DOM sorbent combines high porosity with interconnected macropores, large surface area, and nanosized active particles, advantageous properties that result in excellent desulfurization performance at medium temperatures.[25] Moreover, a stable γ-Fe_2O_3 was found to be easily prepared using a colloidal crystal templating method when silicon was added to the precursors. This work reports the possibility of γ-Fe_2O_3 as a sorbent for H_2S removal at low temperature (20−80 °C) and evaluates the performance of γ-Fe_2O_3 with these novel 3DOM structures. The influence of silicon on the formation of γ-Fe_2O_3 and its performance in H_2S removal is also presented in detail.

2. EXPERIMENTAL SECTION

2.1. Synthesis of 3DOM γ-Fe_2O_3/SiO_2 Sorbent. 3DOM γ-Fe_2O_3/SiO_2 sorbents were synthesized by the colloidal crystal templating method.[25−27] All the materials used and the detailed procedures of preparation can be found in Supporting Information. The obtained 3DOM γ-Fe_2O_3/SiO_2 sorbents were named after their iron-to-silicon mole ratios as FS-1, FS-2, FS-4, FS-8, and FS-16. FE was the prepared sorbent which did not contain silicon in precursors. To compare the sulfur removal performance of the synthesized sorbent, three reference samples—pure analytical reagent γ-Fe_2O_3, α-Fe_2O_3, and a commercial adsorbent HXT-1 provided by Shanxi Clean Company—were used for references in this study. The main component of HXT-1 is amorphous hydrated iron oxide.

2.2. Performance Tests. Sulfur removal evaluations were conducted in a 6 mm inner diameter downflow fixed-bed reactor with a water jacket at atmospheric pressure. The temperature of the reactor was controlled by adjusting the water jacket temperature. The breakthrough experiments were carried under the following conditions unless specially mentioned. The H_2S concentration at the inlet was 500 mg/m^3 balanced with high-purity nitrogen (nitrogen content higher than 99.999% in gas). A 2 cm height of 0.08 g of 3DOM sorbents or reference samples mixed with quartz sands (SiO_2) in the form of small particles of 40−60 mesh was sandwiched in the reactor. The space velocity was 11 671 h^{-1}. The influence of water on H_2S capture was investigated by making the feed gas go through a water saturator at different temperatures (10, 20, 40, and 60 °C with a relative humidity of 10.23%, 18.75%, 55.39%, and 141.04%, respectively). The concentration of H_2S in the gas exiting the reactor was measured continuously using a gas chromatograph equipped with a photometric detector (FPD). The sulfidation test was stopped at the breakthrough point, which was defined by a sulfur content of 1 mg/m^3. Breakthrough sulfur capacity is defined as grams of sulfur captured per 100 g of sorbent at the breakthrough point. The utilization of iron oxide for desulfurization is calculated based on the maximum theoretical sulfur capacity of 60 g per gram of iron oxide.[17] The grain size can be measured by transmission electron microscopy (TEM) or calculated based on the Sherrer formula:

$$D = K\lambda/\beta \cos\theta$$

where D is the average grain size, K the Sherrer constant (0.891), and λ the X-ray wavelength (0.15405 nm). β and θ represent full-width at half-maximum of an observed peak and diffraction angle, respectively.

3. RESULTS AND DISCUSSION

3.1. Characterization of the Synthesized Sorbents. The synthesized sorbents were first analyzed by X-ray diffraction (XRD) measurement to confirm the mineral phase structures. The results are shown in Figure 1a. The references γ-Fe_2O_3 and α-Fe_2O_3 are also characterized; the corresponding XRD patterns are shown in Figure S1 in Supporting Information.

As shown in Figure 1a, characteristic peaks corresponding to γ-Fe_2O_3 were found in all the prepared sorbents except FE, which did not contain silicon in the precursors. The intensities of the peaks were greater with an increase of Fe/Si molar ratio, which suggests an increase in crystal size.[25,28] In addition, it was observed that α-Fe_2O_3[25,27,28] was present in the sorbent FS-16 and was the only mineral phase in the sorbent FE. Obviously, silicon species have a remarkable influence on the crystal form of iron oxide even though they cannot be detected in all the sorbents because of their amorphous state.

Fourier transform infrared (FTIR) spectra of the γ-Fe_2O_3/SiO_2 sorbent are shown in Figure 1b. The strong, broad peak at 3451 cm^{-1} can be assigned to the O−H symmetric and antisymmetric stretching vibrations of the water molecules.[29] The peak at 1635 cm^{-1} can be assigned to the H−O−H bending vibrations. Si−O−Si backbone vibrations at 1126 and 1079 cm^{-1} are associated with the formation of a condensed silica network, and a weak peak associated with noncondensed Si−OH groups at 964 cm^{-1} is also present.[30] The fairly sharp peaks at 640 and 447 cm^{-1} are assigned to Fe−O−Fe.[31] The FTIR analysis indicated the appearance of SiO_2 and that the samples comprised metal oxides doped with silica.

XPS spectra of FS-8 are shown in Figure 2. The binding energies (BEs) of 710.3 and 723.8 eV, in Figure 2a, are characteristic of Fe 2p3/2 and Fe 2p1/2 of Fe_2O_3,[32−34] respectively. These results reveal the existence of Fe_2O_3, which

DOI: 10.1021/acs.iecr.5b01398
Ind. Eng. Chem. Res. 2015, 54, 8469−8478

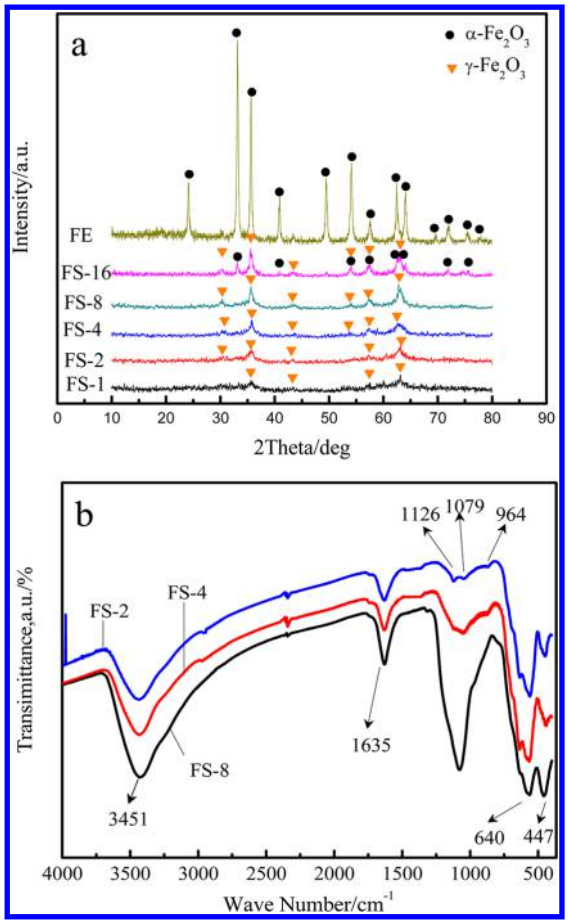

Figure 1. XRD patterns of FS-1, FS-2, FS-4, FS-8, FS-16, and FE (a) and FTIR spectra of FS-2, FS-4, and FS-8 (b).

is in agreement with the XRD result. The BEs of 711.7 and 725.2 eV correspond to the signals of Fe 2p3/2 and Fe 2p1/2 of FeOOH.[32,35,36] The absence of the peak of FeOOH in XRD patterns results from the limited sensitivity of XRD toward the minority species. The BE of O 2p in Fe_2O_3 is 530.5 eV[33,34,37] (in Figure 2b), and 531.7 eV belongs to FeOOH.[32,33] Another BE of 533.4 eV fits best to O 2p of absorbed H_2O.[35] As shown in Figure 2c, the BE of 102.6 eV (SiO_2, O 2p 532.6 eV[38]) is attributed to SiO_2, which agrees with the FTIR results.

Combined with the XRD results, it is known that the silicon in these sorbents is in the form of highly dispersed amorphous SiO_2. These results seem to indicate that two effects arise from the inclusion of silicon. On the one hand, SiO_2 can disperse and inhibit the growth of iron oxide crystals. The higher the content of SiO_2, the smaller the grain size of iron oxide. On the other hand, SiO_2 can help to stabilize the γ-Fe_2O_3 form and hamper its transformation to α-Fe_2O_3 during the calcination process. A similar role for yttrium in the formation of γ-Fe_2O_3 has been reported by Tao et al.[39] Ayyub et al.[40−42] also reported that the transition from γ-Fe_2O_3 to α-Fe_2O_3 phases is size-dependent and that a decrease in particle size seems to improve the stability of γ-Fe_2O_3. Therefore, it is likely that SiO_2 plays a role in hampering the $\gamma-\alpha$ transition by reducing the particle size of γ-Fe_2O_3.

Scanning electron microscopy (SEM) and TEM analyses were carried out to investigate the morphology and structure of the sorbents. As shown in Figure 3, all sorbents exhibit a 3DOM structure that is open and interconnected. These interconnected networks and well-ordered macropores provide greater mass transfer ability and a larger inner surface area. TEM of the sorbents reveals that nanocrystallized particles are formed in the structure with mesopore-sized void spaces between the crystallites. The sizes of the nanocrystallized particles in the sorbents are listed in Table 1. Clearly, the size of the nanocrystallized particles increased with the molar ratio of iron to silicon.

N_2 sorption analyses were performed to determine the surface areas and porous structures of the FS sorbents, and the nitrogen adsorption−desorption isotherms are shown in Figure S2 in Supporting Information. All the sorbents showed a type II isotherm, and a significant increase of N_2 adsorption was observed at pressures beyond 0.8 P/P_0. The results are consistent with those for many 3DOM macroporous materials. Pore distribution indicates the presence of mesopores in the materials. The parameters of the sorbents are summarized in Table 1, showing that the BET surface areas are in the range of 72.1−125.8 m^2/g. The average pore size was in the range of 7.50−9.0 nm and decreased as the Fe/Si molar ratio increased. The texture parameters of reference sorbents are also shown in Table 1.

3.2. Testing of γ-Fe_2O_3 for H_2S Removal. The activity of γ-Fe_2O_3 for H_2S removal was first evaluated in a fixed bed reactor using an analytically pure reagent as reference. The experiment was carried out at a temperature range of 20−80 °C, with typical conditions described in the Experimental Section. Comparative experiments with a commercial sorbent, HXT-1, and reference α-Fe_2O_3 were also conducted under the same conditions. The test results are shown in Figure 4.

As shown in Figure 4a, γ-Fe_2O_3 captured little sulfur at 20 °C with a sulfur capacity of 0.65%, and the breakthrough time at 40 °C, about 25 min, was also very short with the sulfur capacity only 1.43%. However, a much longer breakthrough time could be obtained at higher temperature. At 60 °C, the breakthrough time was about 50 min and a sulfur capacity of 3.24% was achieved. Moreover, the breakthrough time at 80 °C increased significantly to 150 min, and the corresponding sulfur capacity reached 10.58%. The comparative results with reference α-Fe_2O_3 and the commercial sorbent, HXT-1, are shown in Figure 4b, demonstrating that α-Fe_2O_3 has almost no activity for sulfur capture while γ-Fe_2O_3 performed worse than HXT-1 at low temperature but better at higher temperatures.

It has been reported that a lattice diffusion is involved during the interaction of adsorbed H_2S with solid metal oxide.[1,7−10] Lattice diffusion, also termed "ion diffusion" or "the solid-state diffusion", means the ion migration or ion exchange in the lattice of oxide,[43−47] which is required to complete the reaction of metal oxide in the bulk with H_2S. It was reported that at low temperature this lattice diffusion is very hard and that therefore the desulfurization process was controlled by lattice diffusion. However, the mechanisms for the low-temperature diffusion of ions through the solids are still not well-understood.[1,48,49] It is suggested that defect and vacancy may contribute to this diffusion. For example, the vacancy of zinc in ZnO sorbent was found to improve the transfer of ions in the lattice during the reaction of H_2S with ZnO.[1] Kim et al. also reported the great enhancement of vacancies on the diffusivity of ion transport in the bulk of the cathode material.[50]

It is known that γ-Fe_2O_3 has the same inverse spinel crystal structure as Fe_3O_4, but with all the iron cations being in a trivalent state.[15] The charge neutrality of γ-Fe_2O_3 is maintained by the presence of cation vacancies. The effect of cation

DOI: 10.1021/acs.iecr.5b01398
Ind. Eng. Chem. Res. 2015, 54, 8469−8478

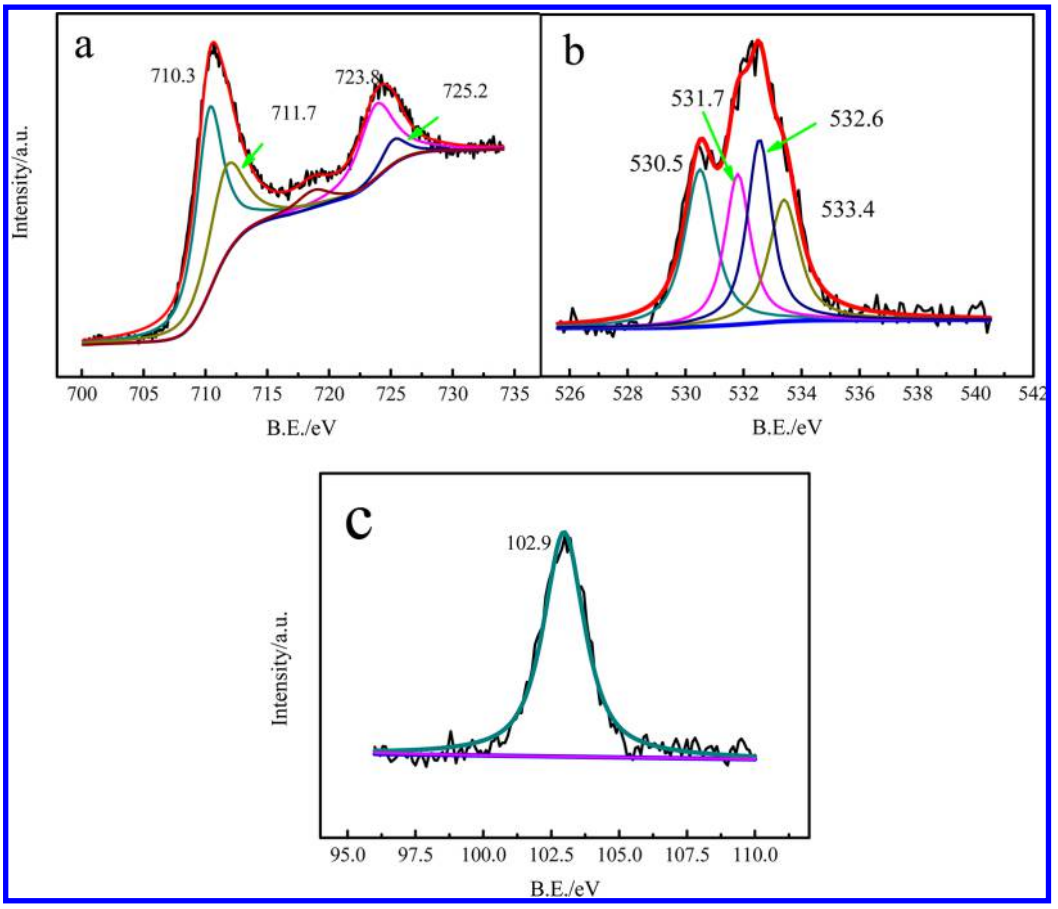

Figure 2. XPS spectra of FS-8: (a) Fe 2p, (b) O 1s, (c) Si 2p.

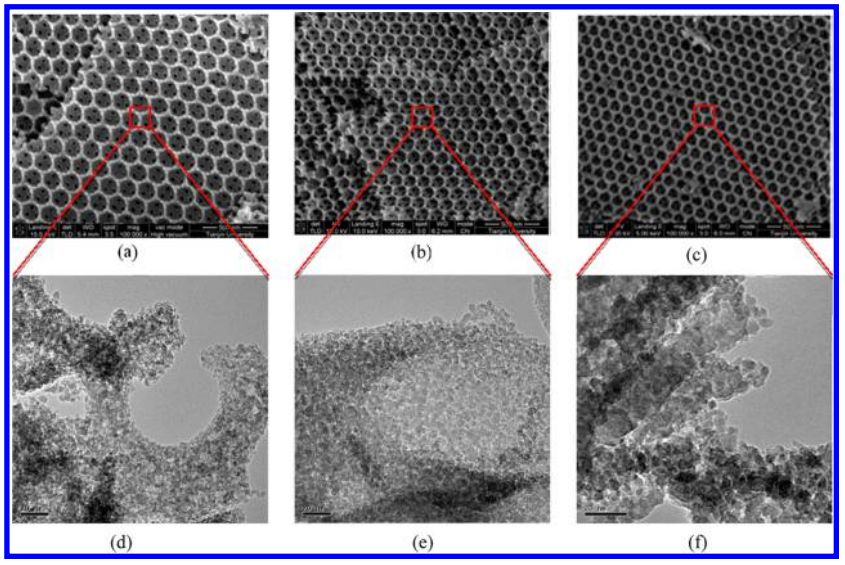

Figure 3. SEM and high-resoltuion TEM (HRTEM) images of 3DOM sorbents. SEM: (a) FS-2, (b) FS-4, and (c) FS-8. HRTEM: (d) FS-2, (e) FS-4, and (f) FS-8.

vacancies on ion transport has been used for efficient sodium ion transport in hollow γ-Fe_2O_3 nanoparticles as a cathode material.[23] In the case of removal of H_2S by γ-Fe_2O_3, the vacancy is also considered to favor the lattice diffusion of ions and thus improves the ability of the material to capture sulfur.

In fact, there are many other factors that could influence the performance of the sorbent. Surface area, density, morphology, and porosity are important,[8−10,13,49] while dispersion of active site, surface acidity and basicity, and rearrangement of the crystal after sulfidation, etc. are also reported to play a significant role.[8−10,25,51] It is well-known that γ-Fe_2O_3 and α-Fe_2O_3 are polymorphs. The former is metastable, whereas the latter is very stable. They have different crystal structures and thus have different physical and chemical properties which therefore lead to different performance.[15,52,53] Reference γ-Fe_2O_3 has lower density (4.87 g/m^3),[15] larger surface area, and

DOI: 10.1021/acs.iecr.5b01398
Ind. Eng. Chem. Res. 2015, 54, 8469−8478

Table 1. Texture Parameters of 3DOM and Reference Sorbents

sample	S_{BET} (m^2/g)	average pore size (nm)	grain size (nm)
FS-1	125	7.50	3.0
FS-2	120	8.28	4.6
FS-4	120	9.00	6.3
FS-8	113	8.21	8.1
FS-16	72	8.26	9.9
γ-Fe_2O_3	82	9.75	11.6
α-Fe_2O_3	36	2.44	54.2
HXT-1	87	3.70	—

[a]The grain size of FS-16 and α-Fe_2O_3 was calculated based on the Sherrer formula.

smaller grain size than that of α-Fe_2O_3, as shown in Table 1, which results in a much better performance in H_2S capture, as compared with that of reference α-Fe_2O_3 in this study.

3.3. Evaluation of 3DOM γ-Fe_2O_3/SiO_2 Sorbents for H_2S Removal. The desulfurization performance of the synthesized 3DOM sorbents FS-1, FS-2, FS-4, FS-8, and FS-16 were examined at 80 °C. Before the experiments, a blank experiment was carried showing that 3DOM SiO_2 did not contribute to H_2S removal. Figure 5a shows the breakthrough curves for H_2S removal compared with the results for γ-Fe_2O_3. It can be seen that γ-Fe_2O_3 and all the 3DOM γ-Fe_2O_3/SiO_2 sorbents achieve a very low exit H_2S concentration (<0.1 mg/m^3) and a very sharp breakthrough curve. With the exception of FS-1, all sorbents with a 3DOM structure show better performance than reference γ-Fe_2O_3 and HXT-1, indicating a very positive effect of the 3DOM structure on the sorbents. FS-8 has the longest breakthrough time of 9.4 h and the highest sulfur capacity of 40.61% among these sorbents (Figure 5b). Because of its low iron oxide content, FS-1 performs very poorly compared to the other 3DOM sorbents. In contrast, although the Fe_2O_3 content of FS-16 is the highest of these sorbents, a very short breakthrough time and low capacity were observed. This result could be attributed to the presence of α-Fe_2O_3 as revealed by XRD. The very poor adsorption capacity of α-Fe_2O_3 (as shown in Figure 5b) cannot contribute to desulfurization.

The utilization of iron oxide for desulfurization by these sorbents is shown in Figure 5b. It is apparent that all of the 3DOM sorbents have higher utilization than γ-Fe_2O_3 and α-Fe_2O_3. Desulfurization is a reaction between the metal oxide and hydrogen sulfide, and pore-closure will occur during the process because of the larger volume of the product compared to that of the reactant.[54,55] Consequently, increasing diffusion resistance in the pores of the sorbent makes it difficult to react completely with the inner active sites, resulting in a low utilization of active components. In contrast, the 3DOM sorbents, characterized by many interconnected macropores and mesopores in the skeleton, can significantly alleviate diffusion resistance and greatly increase accessibility to the inner part of the sorbent for more complete reaction. Furthermore, the very large surface area, together with the nanosized active particles, provides far more active sites for H_2S removal. It can be concluded that the combination of the

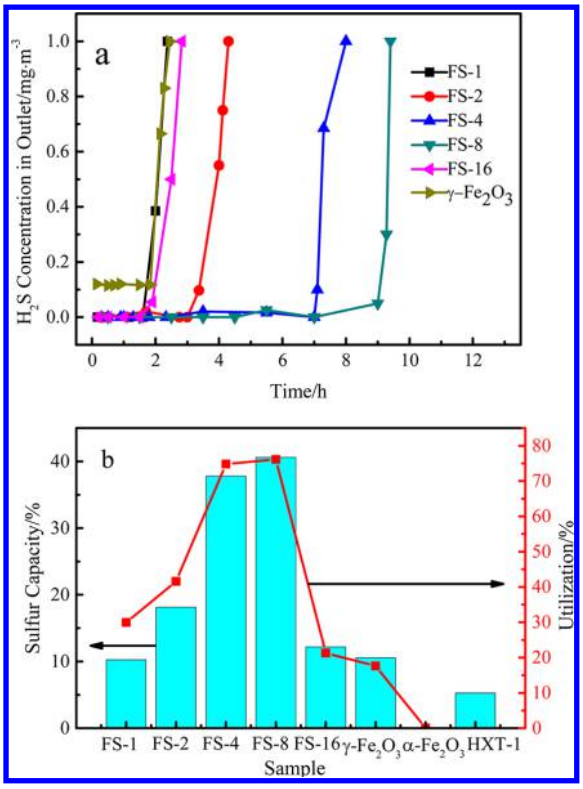

Figure 5. Breakthrough curves (a) and sulfur capacity and utilization (b) of 3DOM and reference sorbents at 80 °C.

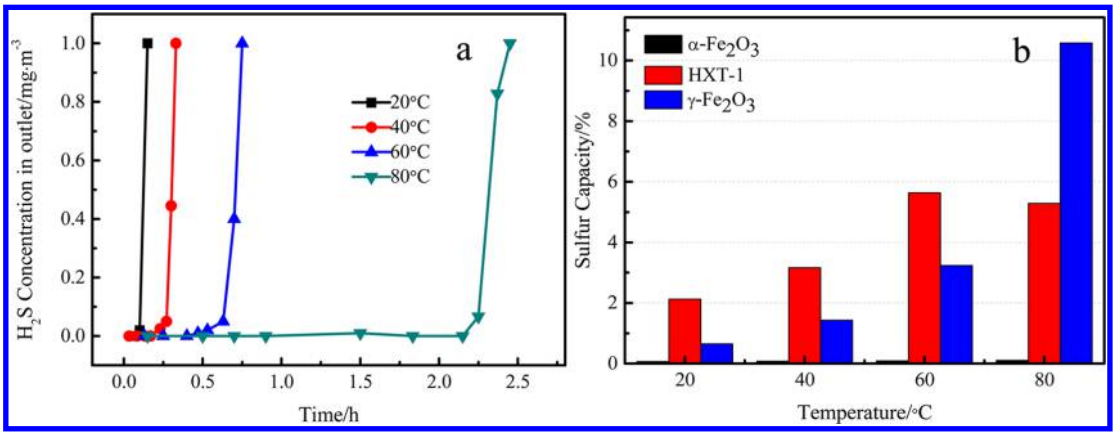

Figure 4. Breakthrough curves of reference γ-Fe_2O_3 at different temperatures (a) and sulfur capacity of reference γ-Fe_2O_3, α-Fe_2O_3, and HXT-1 at different temperatures (b).

DOI: 10.1021/acs.iecr.5b01398
Ind. Eng. Chem. Res. 2015, 54, 8469−8478

advantageous features of high porosity with interconnected macropores, large surface area, and nanosized active particles, contribute to the very high utilization of γ-Fe_2O_3 in the 3DOM sorbents.

In addition, to confirm the structural changes during sulfidition, the sulfided 3DOM sorbents were characterized by SEM and nitrogen adsorption. Compared with the fresh 3DOM sorbents, although the surface area decreased (shown in Table S1 in Supporting Information), the 3DOM structure was maintained very well (shown in Figure S3 in Supporting Information).

The performance of 3DOM γ-Fe_2O_3/SiO_2 sorbent for H_2S removal was also tested at different temperatures using sample FS-8. The breakthrough curves are shown in Figure 6. It can be seen that the breakthrough times of the absorbent were extremely short at 20 and 40 °C, indicating very poor activity at low temperature. However, the activity increased remarkably as the temperature was increased to 60 and 80 °C, with breakthrough times of 3.5 and 9.4 h, respectively. This temperature sensitivity is similar to that for γ-Fe_2O_3, shown in Figure 4. When the breakthrough curves of γ-Fe_2O_3 and FS-8 at different temperatures are compared, it can be seen that FS-8 performs better than γ-Fe_2O_3 at temperatures above 60 °C.

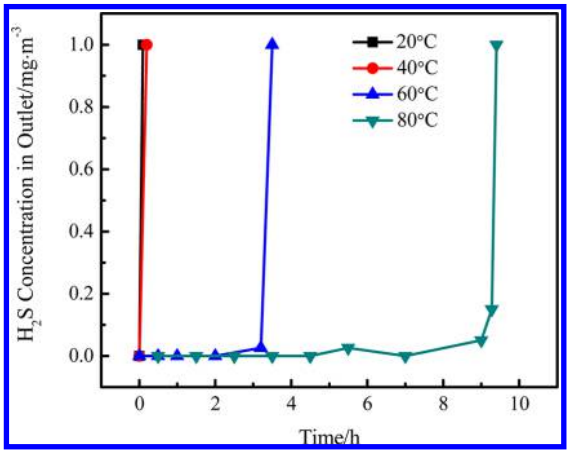

Figure 6. Breakthrough curves of FS-8 at different temperatures.

3.4. Influence of Moisture on H_2S Removal. H_2S adsorption tests of reference γ-Fe_2O_3 were also carried out in moist conditions, in which the feed gas was humidified by bubbling through a water bath at the temperatures of 10, 20, 40, and 60 °C with a relative humidity of 10.23%, 18.75%, 55.39%, and 141.04%, respectively. The influence of humidity on H_2S removal and the corresponding breakthrough sulfur capacities at different water content are shown in Figure 7. The results reveal that the water content in the feed gas has a remarkable influence on H_2S removal. The performance of reference γ-Fe_2O_3 was best when relative humidity was 10.23%, with a breakthrough time of 3.4 h and sulfur capacity of 14.03%. It has been reported that water increases hydrogen sulfide uptake by promoting dissociation of H_2S.[56] However, increasing the water content further led to a negative effect on H_2S adsorption. For example, when relative humidity was 141.04%, the breakthrough capacity was only 4.95%. This is because too much water can block the interior pores of the material, prohibiting the diffusion of H_2S through the sorbent.

The desulfurization behavior of the 3DOM γ-Fe_2O_3/SiO_2 sorbent was also evaluated in a moist atmosphere (RH = 10.23%) at 80 °C, where a negative influence on H_2S uptake was found. Another experiment, in which FS-8 was preheated at 200 °C for 2 h, resulted in almost no H_2S adsorption activity. It is suggested that, because of its very porous nature, 3DOM γ-Fe_2O_3/SiO_2 actually has adsorbed water molecules on the surface, which is in agreement with the XPS results. This adsorbed water favors the promotion of H_2S adsorption.

3.5. Regeneration of 3DOM γ-Fe_2O_3/SiO_2 Sorbents. Regeneration is generally required to reduce the cost of desulfurization. Therefore, the regenerability of the 3DOM γ-Fe_2O_3/SiO_2 sorbents was also examined in this study. Considering the transformation temperature of γ-Fe_2O_3, the regeneration of the sulfide sorbents was tested at medium temperature using 5% O_2 in nitrogen with a flow of 200 mL/min. The regeneration was initially conducted at 300 °C. Once the level of SO_2 in the outflow was below 5 mg/m^3, the temperature was raised to 400 °C to continue regeneration. A poor sulfur capture performance after regeneration, confirmed by an experiment (shown in Figure 8b) which shows that the sulfur capacity of the regenerated sorbent was only 11.28%, less than one-third of that of the fresh material. The XRD analysis (shown in Figure 8a) of the regenerated sorbent shows that iron oxide was present in both the γ and α forms although no sulfur species were found after regeneration. Furthermore, compared with the fresh sorbent, the surface area of the regenerated FS-8 sorbent decreased significantly, from 113 to 78 m^2/g, as revealed by nitrogen adsorption characterization. The α-Fe_2O_3 formed during regeneration, together with the

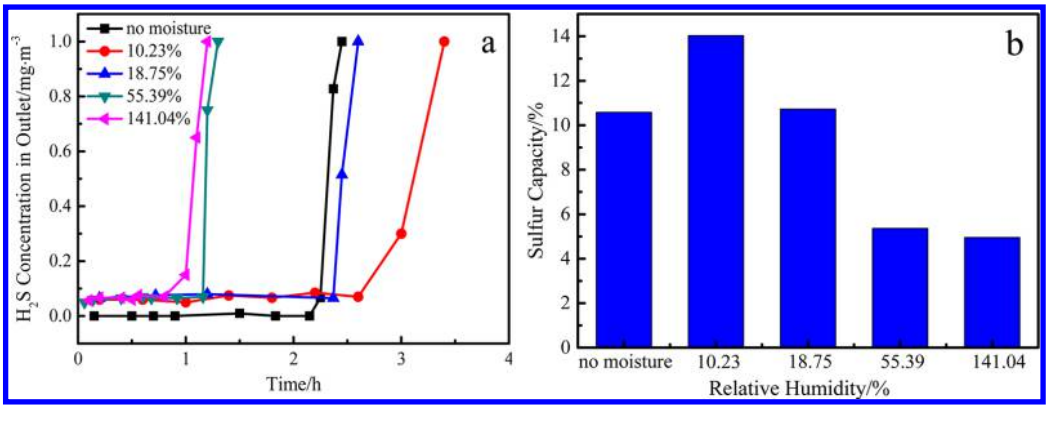

Figure 7. Breakthrough curves (a) and sulfur capacity (b) of reference γ-Fe_2O_3 at 80 °C with different relative humidity.

DOI: 10.1021/acs.iecr.5b01398
Ind. Eng. Chem. Res. 2015, 54, 8469−8478

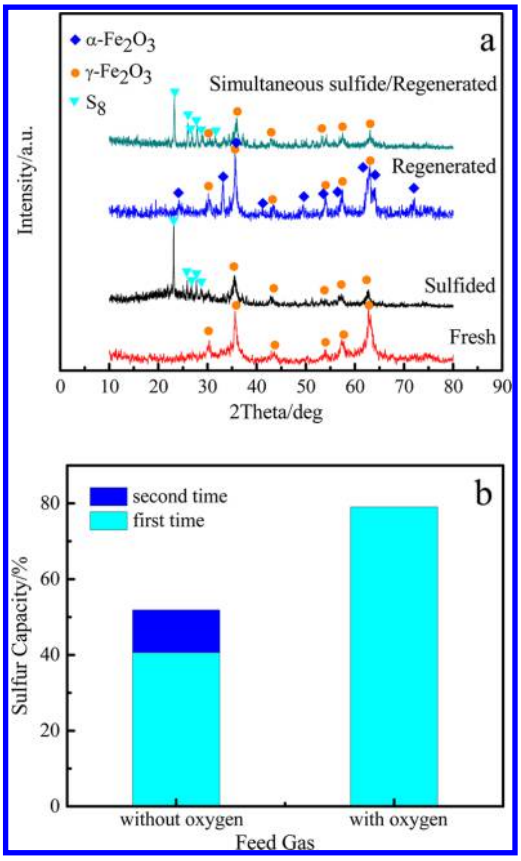

Figure 8. XRD patterns of fresh, sulfided, and regenerated FS-8 (a) and sulfur capacity of continuous and intermittent desulfurization (b).

decreased surface area, led to the poor performance of regenerated FS-8.

A revivifying in situ method (simultaneous sulfidation and regeneration), which can result in a much simpler and more economical process of desulfurization by hydrated iron oxide, was tried on FS-8 for H_2S removal. Specifically, a mixture of oxygen (5%) and 500 mg/m^3 H_2S in nitrogen was introduced to the reactor for sulfidation of FS-8 at 80 °C. The results, shown in Figure S4 in Supporting Information and Figure 8b, illustrate that a much longer breakthrough time of 18.23 h and much higher capacity of 79.1% can be obtained, which is almost twice that observed when oxygen is absent from the inlet gas. Elemental sulfur was clearly seen on the surface of the sorbent, which was also revealed by XRD analysis (Figure 8a).

3.6. Reactions Involved in Removal of H_2S by γ-Fe_2O_3.

It is considered that the reaction between γ-Fe_2O_3 and H_2S can occur through a direct exchange of sulfur and oxygen ions to form sulfide and water.

$$Fe_2O_3 + 3H_2S \rightarrow Fe_2S_3 + 3H_2O \quad (1)$$

Because of the presence of the other active site FeOOH (in Table 2)[32,33,35,38] on the surface, as revealed in Figure 9, H_2S could also react with FeOOH:

$$2FeOOH + 3H_2S \rightarrow Fe_2S_3 + 4H_2O \quad (2)$$

XRD of the spent sorbent FS-8, as depicted in Figure 8a, showed that compared to the fresh material, new peaks corresponding to elemental sulfur were present. No evidence of Fe_2S_3 was detected. The existence of elemental sulfur as well as γ-Fe_2O_3 in the exhausted sorbent indicates that regeneration

Table 2. XPS Binding Energy (in Electronvolts) of Fresh and Sulfided FS-8[32−38,57,58]

material	Fe 2p3/2, Fe 2p1/2	O 2p	S 2p3/2, S 2p1/2	Si 2p
Fe_2O_3	710.3, 723.8	530.5	—	—
FeOOH	711.7, 725.2	531.7	—	—
SiO_2	—	532.6	—	102.9
H_2O	—	533.4	—	—
$Fe_2(SO_4)_3$	713.4, 726.9	532.1	168.3, 169.3	—
FeS_2	710.3, 723.8	—	162.2	—
Fe_3S_4	708.9, 722.5	—	161.4	—
S_8	—	—	163.7, 164.2	—

can occur when the sorbent is exposed to air during sample preparation for XRD characterization.

$$2Fe_2S_3 + 3O_2 \rightarrow 2Fe_2O_3 + 3/4S_8 \quad (3)$$

Considering the desulfurization behavior of γ-Fe_2O_3 under the atmosphere containing oxygen, it is suggested that the overall process of desulfurization in the presence of oxygen in the feed gas is that described in eq 4, which is the combination of eqs 1 and 3:

$$2H_2S + O_2 \rightarrow 2H_2O + 1/4S_8 \quad (4)$$

Although Fe_2S_3 was not found in the spent sorbent, full regeneration cannot be concluded. The spent FS-8 sorbent was further examined by XPS. As shown in Figure 9, no evidence for the presence of Fe_2S_3 could be found, but elemental sulfur,[33,57] Fe_3S_4,[58] $Fe_2(SO_4)_3$,[33,34,58] and FeS_2[33,58] (in Table 2) were detected. The reason why the latter three species could not be found in the XRD spectra is that they may have been present in very small amounts or in an amorphous form. TG characterization of the spent sorbent, carried out in N_2 atmosphere at a heating rate of 10 °C/min (shown in Figure S5 in Supporting Information), indicated a sharp weight decrease at 250 °C due to the evaporation of elemental sulfur that was formed when the spent sorbent was exposed to air. Above 270 °C there was no obvious weight loss, even at 480 °C, which is the decomposition temperature of ferric sulfate. The results indicate that very little ferric sulfate was formed on the sorbent.

On the basis of these results, it is possible to conclude that Fe_2S_3 might convert to FeS_2 and Fe_3S_4[16] because of its thermodynamic instability.

$$2Fe_2S_3 \rightarrow FeS_2 + Fe_3S_4 \quad (5)$$

FeS_2 can also be converted into $Fe_2(SO_4)_3$, as described in eq 6, when O_2 and H_2O are present[45]

$$4FeS_2 + 15O_2 + 2H_2O \rightarrow 2Fe_2(SO_4)_3 + 2H_2SO_4 \quad (6)$$

Equations 1−6 represent a suggested mechanism for the desulfurization process. The principal reaction during desulfurization in the absence of oxygen should be eq 1, whereas eqs 1, 3, and 4 are mainly involved when oxygen is present in the feed gas. However, depending on operating conditions such as temperature or composition of the feed, other reactions may occur.

4. CONCLUSIONS

3DOM γ-Fe_2O_3/SiO_2 sorbents were successfully synthesized using colloidal crystal templating method when silicon was added to the precursors. SiO_2 was in an amorphous state and highly dispersed. It enhanced the dispersion of Fe_2O_3, which

DOI: 10.1021/acs.iecr.5b01398
Ind. Eng. Chem. Res. 2015, 54, 8469−8478

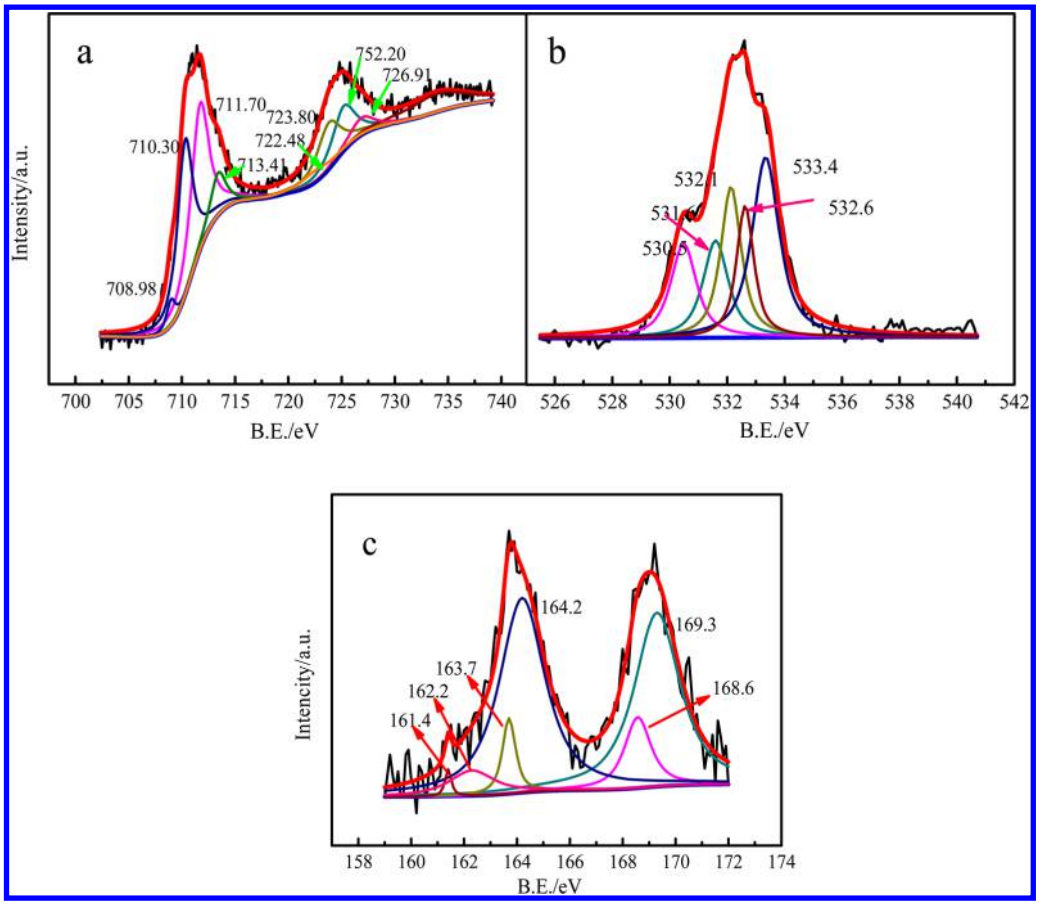

Figure 9. XPS spectra of the sulfided FS-8: (a) Fe 2p, (b) O 1s, and (c) S 2p.

stabilized the γ-Fe_2O_3 and hindered its transformation to α-Fe_2O_3 during calcination. The performance of 3DOM γ-Fe_2O_3/SiO_2 sorbents and analytical pure reference γ-Fe_2O_3 for H_2S capture were evaluated, and the results were compared with that of reference α-Fe_2O_3 as well as the commercial sorbent HXT-1. It was also found that γ-Fe_2O_3 has an activity that is enhanced compared to that of HXT-1 for H_2S capture at temperatures over 60 °C, whereas α-Fe_2O_3 has little activity. The vacancy site in the lattice of γ-Fe_2O_3 facilitates the ion diffusion. Furthermore, reference γ-Fe_2O_3 also has the lower density, larger surface area, and smaller grain size than that of α-Fe_2O_3. Therefore, reference γ-Fe_2O_3 has much better performance in H_2S capture, as compared with that of reference α-Fe_2O_3. Moreover, 3DOM γ-Fe_2O_3/SiO_2 sorbents with the mole ratios of iron to silicon ranged at 2−8 exhibited better performance than reference γ-Fe_2O_3. It is believed that this is contributed by its unique properties of 3DOM: very high porosity with interconnected macropore, large surface area, and nanosized active particles. Meanwhile, it was also found that FS-8 had the highest sulfur capacity of 40.61%, as well as the highest utilization of 76.15%. Moist conditions favored H_2S removal. It was also found that conventional regeneration method with air at high temperature was not ideal for γ-Fe_2O_3/SiO_2 sorbents regeneration. However, through an in situ regeneration process by adding O_2 in the feed stream (desulfurization and regeneration occur at the same time), a breakthrough sulfur capacity of 79.1% of FS-8 was achieved.

■ ASSOCIATED CONTENT

Supporting Information

The Supporting Information is available free of charge on the ACS Publications website at DOI: 10.1021/acs.iecr.5b01398.

Materials and synthesis of 3DOM γ-Fe_2O_3/SiO_2 sorbent, XRD patterns of γ-Fe_2O_3 and α-Fe_2O_3, nitrogen adsorption and desorption isotherms, SEM image of sulfided FS-8 sorbent, breakthrough curves of FS-8 with and without oxygen in feed gas, TG curves of sulfided FS-8, and texture parameters of spent 3DOM sorbents. (PDF)

■ AUTHOR INFORMATION

Corresponding Author

*Tel.: 0086-351-6010530. Fax: 0086-351-6010530. E-mail: fanhuiling@tyut.edu.cn.

Notes

The authors declare no competing financial interest.

■ ACKNOWLEDGMENTS

This work was financially supported by National Cooperation Project of Shanxi Province (2014081007-3) and National Nature Science Fundamental (51272170). We deeply appreciate Mr. Zhen Tian, from Service Center of Micromeritics (Shanghai) Ltd., for very helpful discussion about nitrogen adsorption results.

DOI: 10.1021/acs.iecr.5b01398
Ind. Eng. Chem. Res. 2015, 54, 8469−8478

REFERENCES

(1) Stirling, D. *The Sulfur Problem: Cleaning Up Industrial Feedstocks*; Royal Society of Chemistry: Cambridge, 2000.

(2) Jou, F. Y.; Mather, A. E.; Otto, F. D. Solubility of Hydrogen Sulfide and Carbon Dioxide in Aqueous Methyldiethanolamine Solutions. *Ind. Eng. Chem. Process Des. Dev.* **1982**, *21*, 539.

(3) Yin, F. K.; Yu, J. L.; Dou, J. X.; Gupta, S.; Moghtaderi, B.; Lucas, J. Sulfidation of Iron-Based Sorbents Supported on Activated Chars during the Desulfurization of Coke Oven Gases: Effects of Mo and Ce Addition. *Energy Fuels* **2014**, *28*, 2481.

(4) Kumar, P.; Sung, C. Y.; Muraza, O.; Cococcioni, M.; Al Hashimi, S.; McCormick, A.; Tsapatsis, M. H_2S Adsorption by Ag and Cu Ion Exchanged Faujasites. *Microporous Mesoporous Mater.* **2011**, *146*, 127.

(5) Garces, H. F.; Galindo, H. M.; Garces, L. J.; Hunt, J.; Morey, A.; Suib, S. L. Low Temperature H_2S Dry-desulfurization with Zinc Oxide. *Microporous Mesoporous Mater.* **2010**, *127*, 190.

(6) Song, H. S.; Park, M. G.; Kwon, S. J.; Yi, K. B.; Croiset, E.; Chen, Z.; Nam, S. C. Hydrogen Sulfide Adsorption on Nano-sized Zinc Oxide/reduced Graphite Oxide Composite at Ambient Condition. *Appl. Surf. Sci.* **2013**, *276*, 646.

(7) Carnes, C. L.; Klabunde, K. J. Unique Chemical Reactivities of Nanocrystalline Metal Oxides toward Hydrogen Sulfide. *Chem. Mater.* **2002**, *14*, 1806.

(8) Polychronopoulou, K.; Fierro, J. L. G.; Efstathiou, A. M. Novel Zn-Ti-based Mixed Metal Oxides for Low-temperature Adsorption of H_2S from Industrial Gas Streams. *Appl. Catal., B* **2005**, *57*, 125.

(9) Polychronopoulou, K.; Galisteo, F. C.; Granados, M. L.; Fierro, J. L. G.; Bakas, T.; Efstathiou, A. M. Novel Fe-Mn-Zn-Ti-O Mixed-metal Oxides for the Low-Temperature Removal of H_2S from Gas Streams in the Presence of H_2, CO_2, and H_2O. *J. Catal.* **2005**, *236*, 205.

(10) Polychronopoulou, K.; Efstathiou, A. M. Effects of Sol-Gel Synthesis on 5Fe-15Mn-40Zn-40Ti-O Mixed Oxide Structure and its H_2S Removal Efficiency from Industrial Gas Streams. *Environ. Sci. Technol.* **2009**, *43*, 4367.

(11) Baird, T.; Campbell, K. C.; Holliman, P. J.; Hoyle, R.; Stirling, D.; Williams, B. P. Structural and Morphological Studies of Iron Sulfide. *J. Chem. Soc., Faraday Trans.* **1996**, *92*, 445.

(12) Skrzypski, J.; Bezverkhyy, I.; Heintz, O.; Bellat, J. P. Low Temperature H_2S Removal with Metal-doped Nanostructure ZnO Sorbents: Study of the Origin of Enhanced Reactivity in Cu-containing Materials. *Ind. Eng. Chem. Res.* **2011**, *50*, 5714.

(13) Baird, T.; Campbell, K. C.; Holliman, P. J.; Hoyle, R.; Noble, G.; Stirling, D.; Williams, B. P. Mixed Cobalt-iron Oxide Absorbents for Low-temperature Gas Desulfurisation. *J. Mater. Chem.* **2003**, *13*, 2341.

(14) Miura, K.; Mae, K.; Inoue, T.; Yoshimi, T.; Nakagawa, H.; Hashimoto, K. Simultaneous Removal of Carbonyl Sulfide and Hydrogen Sulfide from Coke Oven Gas at Low Temperature by Iron Oxide. *Ind. Eng. Chem. Res.* **1992**, *31*, 415.

(15) Cornell, R. M.; Schwertmann, U. *The Iron Oxides: Structure, Properties, Reactions, Occurrences and Uses*; WILEY-VCH Verlag Gmbh & Co. KGaA: Weinheim, 2006.

(16) Davydov, A.; Chuang, K. T.; Sanger, A. R. Mechanism of H_2S Oxidation by Ferric Oxide and Hydroxide Surfaces. *J. Phys. Chem. B* **1998**, *102*, 4745.

(17) Kohl, A. L.; Richard, N. *Gas Purification*; Gulf Professional Publishing: Amsterdam, 1997.

(18) Gong, Z. J.; Tian, Y. Y.; Li, W. H.; Xu, Z. G. Study on the Preparation Principle of Iron Oxides and Desulfurization Activity. *Coal Convers.* **2006**, *29*, 75.

(19) Fang, J.; Kumbhar, A.; Zhou, W. L.; Stokes, K. L. Nanoneedles of Maghemite Iron Oxide Prepared from a Wet Chemical Route. *Mater. Res. Bull.* **2003**, *38*, 461.

(20) Bate, G. Magnetic Recording Materials since 1975. *J. Magn. Magn. Mater.* **1991**, *100*, 413.

(21) Teja, A. S.; Koh, P. Y. Synthesis, Properties and Applications of Magnetic Iron Oxide Nanoparticles. *Prog. Cryst. Growth Charact. Mater.* **2009**, *55*, 22.

(22) Basak, S.; Rane, K. S.; Biswas, P. Hydrazine-assisted, Low-temperature Aerosol Pyrolysis Method to Synthesize γ-Fe_2O_3. *Chem. Mater.* **2008**, *20*, 4906.

(23) Koo, B.; Chattopadhyay, S.; Shibata, T.; Prakapenka, V. B.; Johnson, C. S.; Rajh, T.; Shevchenko, E. V. Intercalation of Sodium Ions into Hollow Iron Oxide Nanoparticles. *Chem. Mater.* **2013**, *25*, 245.

(24) Chhabra, V.; Ayyub, P.; Chattopadhyay, S.; Maitra, A. N. Preparation of Acicular γ-Fe_2O_3 Particles from a Microemulsion-mediated Reaction. *Mater. Lett.* **1996**, *26*, 21.

(25) Fan, H. L.; Sun, T.; Zhao, Y. P.; Shangguan, J.; Lin, J. Y. Three-dimensionally Ordered Macroporous Iron Oxide for Removal of H_2S at Medium Temperatures. *Environ. Sci. Technol.* **2013**, *47*, 4859.

(26) Chen, X. Q.; Li, Z. S. J.; Ye, H.; Zou, Z. G. Forced Impregnation Approach to Fabrication of Large-area, Three-dimensionally Ordered Macroporous Metal Oxides. *Chem. Mater.* **2010**, *22*, 3583.

(27) Sun, T.; Fan, H. L.; Shangguan, J.; Liu, S. X.; Chen, Z. H.; Zhang, L. Preparation of Three-dimensionally Ordered Macroporous Iron Oxide Desulfurizer. *J. China Coal Soc.* **2011**, *36*, 1538.

(28) Ma, X. D.; Sun, H. W.; Sun, Q.; Guo, H. W.; Fan, B.; Zhao, S. Hierarchically Porous Fe_2O_3/CuO Composite Monoliths: Synthesis and Characterization. *J. Nat. Gas Chem.* **2010**, *19*, 589.

(29) Wang, X.; Jia, J.; Zhao, L.; Sun, T. Chemisorption of Hydrogen Sulphide on Zinc Oxide Modified Aluminum-substituted SBA-15. *Appl. Surf. Sci.* **2008**, *254*, 5445.

(30) Wang, X.; Sun, T.; Yang, J.; Zhao, L.; Jia, J. Low-temperature H_2S Removal from Gas Streams with SBA-15 Supported ZnO Nanoparticles. *Chem. Eng. J.* **2008**, *142*, 48.

(31) Maity, D.; Agrawal, D. C. Synthesis of Iron Oxide Nanoparticles under Oxidizing Environment and their Stabilization in Aqueous and Non-aqueous Media. *J. Magn. Magn. Mater.* **2007**, *308*, 46.

(32) Baltrusaitis, J.; Cwiertny, D. M.; Grassian, V. H. Adsorption of Sulfur Dioxide on Hematite and Goethite Particle Surfaces. *Phys. Chem. Chem. Phys.* **2007**, *9*, 5542.

(33) Galicia, P.; Batina, N.; González, I. The Relationship between the Surface Composition and Electrical Properties of Corrosion Films Formed on Carbon Steel in Alkaline Sour Medium: an XPS and EIS Study. *J. Phys. Chem. B* **2006**, *110*, 14398.

(34) Fu, H. B.; Wang, X.; Wu, H. B.; Yin, Y.; Chen, J. M. Heterogeneous Uptake and Oxidation of SO_2 on Iron Oxides. *J. Phys. Chem. C* **2007**, *111*, 6077.

(35) Bonnissel-Gissinger, P.; Alnot, M.; Ehrhardt, J. J.; Behra, P. Surface Oxidation of Pyrite as a Function of pH. *Environ. Sci. Technol.* **1998**, *32*, 2839.

(36) Rao, P. M.; Zheng, X. Unique Magnetic Properties of Single Crystal γ-Fe_2O_3 Nanowires Synthesized by Flame Vapor Deposition. *Nano Lett.* **2011**, *11*, 2390.

(37) McIntyre, N. S.; Zetaruk, D. G. X-ray Photoelectron Spectroscopic Studies of Iron Oxides. *Anal. Chem.* **1977**, *49*, 1521.

(38) Barr, T. L. An ESCA Study of the Termination of the Passivation of Elemental Metals. *J. Phys. Chem.* **1978**, *82*, 1801.

(39) Tao, S. W.; Liu, X. Q.; Chu, X. F.; Shen, Y. S. Preparation and Properties of γ-Fe_2O_3 and Y_2O_3 Doped γ-Fe_2O_3 by a Sol-gel Process. *Sens. Actuators, B* **1999**, *61*, 33.

(40) Ayyub, P.; Multani, M.; Barma, M.; Palkar, V. R.; Vijayaraghavan, R. Size-induced Structural Phase Transitions and Hyperfine Properties of Microcrystalline Fe_2O_3. *J. Phys. C: Solid State Phys.* **1988**, *21*, 2229.

(41) Cannas, C.; Concas, G.; Gatteschi, D.; Musinu, A.; Piccaluga, G.; Sangregorio, C. How to Tailor Maghemite Particle Size in γ-Fe_2O_3-SiO_2 Nanocomposites. *J. Mater. Chem.* **2002**, *12*, 3141.

(42) Cannas, C.; Gatteschi, D.; Musinu, A.; Piccaluga, G.; Sangregorio, C. Structural and Magnetic Properties of Fe_2O_3 Nanoparticles Dispersed over a Silica Matrix. *J. Phys. Chem. B* **1998**, *102*, 7721.

(43) Fan, H. L.; Li, Y. X.; Li, C. H.; Guo, H. X.; Xie, K. C. The Apparent Kinetics of H_2S Removal by Zinc Oxide in the Presence of Hydrogen. *Fuel* **2002**, *81*, 91.

DOI: 10.1021/acs.iecr.5b01398
Ind. Eng. Chem. Res. 2015, 54, 8469−8478

(44) Davidson, J. M.; Lawrie, C. H.; Sohail, K. Kinetics of the Absorption of Hydrogen Sulfide by High Purity and Doped High Surface Area Zinc Oxide. *Ind. Eng. Chem. Res.* **1995**, *34*, 2981.
(45) Davidson, J. M.; Sohail, K. A Drifts Study of the Surface and Bulk Reactions of Hydrogen Sulfide with High Surface Area Zinc Oxide. *Ind. Eng. Chem. Res.* **1995**, *34*, 3675.
(46) Neveux, L.; Chiche, D.; Bazer-Bachi, D.; Favergeon, L.; Pijolat, M. New Insight on the ZnO Sulfidation Reaction: Evidences for an Outward Growth Process of the ZnS Phase. *Chem. Eng. J.* **2012**, *181*, 508.
(47) Fuertes, A. B.; Velasco, G.; Fuente, E.; Alvarez, T. Study of the Direct Sulfation of Limestone Particles at High CO_2 Partial Pressures. *Fuel Process. Technol.* **1994**, *38*, 181.
(48) Baird, T.; Campbell, K. C.; Holliman, P. J.; Hoyle, R. W.; Huxam, M.; Stirling, D.; Williams, B. P.; Morris, M. Cobalt-zinc Oxide Absorbents for Low Temperature Gas Desulfurisation. *J. Mater. Chem.* **1999**, *9*, 599.
(49) Jiang, D. H.; Su, L. H.; Ma, L.; Yao, N.; Xu, X. L.; Tang, H. D.; Li, X. N. Cu-Zn-Al Mixed Metal Oxides Derived from Hydroxycarbonate Precursors for H_2S Removal at Low Temperature. *Appl. Surf. Sci.* **2010**, *256*, 3216.
(50) Kim, G.; Wang, S.; Jacobson, A. J.; Reimus, L.; Brodersen, P.; Mims, C. A. Rapid Oxygen Ion Diffusion and Surface Exchange Kinetics in $PrBaCo_2O_{5+x}$ with a Perovskite Related Structure and Ordered A Cations. *J. Mater. Chem.* **2007**, *17*, 2500.
(51) Fan, H. L.; Shangguan, J.; Liang, L. T.; Li, C. H.; Lin, J. Y. A Comparative Study of the Effect of Clay Binders on Iron Oxide Sorbent in the High-temperature Removal of Hydrogen Sulfide. *Process Saf. Environ. Prot.* **2013**, *91*, 235.
(52) Mou, X. L.; Wei, X. J.; Li, Y.; Shen, W. J. Tuning Crystal-phase and Shape of Fe_2O_3 Nanoparticles for Catalytic Applications. *CrystEngComm* **2012**, *14*, 5107.
(53) Galbreath, K. C.; Zygarlicke, C. J.; Tibbetts, J. E.; Schulz, R. L.; Dunham, G. E. Effects of NO_x, α-Fe_2O_3, γ-Fe_2O_3, and HCl on Mercury Transformations in a 7-kW Coal Combustion System. *Fuel Process. Technol.* **2005**, *86*, 429.
(54) Silaban, A.; Harrison, D. P.; Berggren, M. H.; Jha, M. C. The Reactivity and Durability of Zinc Ferrite High Temperature Desulfurization Sorbents. *Chem. Eng. Commun.* **1991**, *107*, 55.
(55) Efthimiadis, E. A.; Sotirchos, S. V. Effects of Pore Structure on the Performance of Coal Gas Desulfurization Sorbents. *Chem. Eng. Sci.* **1993**, *48*, 1971.
(56) Coskun, I.; Tollefson, E. L. Oxidation of Low Concentrations of Hydrogen Sulfide over Activated Carbon. *Can. J. Chem. Eng.* **1980**, *58*, 72.
(57) Collins, R. J.; Sukenik, C. N. Sulfonate-functionalized, Siloxane-anchored, Self-assembled Monolayers. *Langmuir* **1995**, *11*, 2322.
(58) Descostes, M.; Mercier, F.; Thromat, N.; Beaucaire, C.; Gautier-Soyer, M. Use of XPS in the Determination of Chemical Environment and Oxidation State of Iron and Sulfur Samples: Constitution of a Data Basis in Binding Energies for Fe and S Reference Compounds and Applications to the Evidence of Surface Species of an Oxidized Pyrite in a Carbonate Medium. *Appl. Surf. Sci.* **2000**, *165*, 288.

DOI: 10.1021/acs.iecr.5b01398
Ind. Eng. Chem. Res. 2015, 54, 8469−8478